

Superconducting LaPtH₆ with triatomic hydrogen units

Takahiro Ishikawa,^{1,*} Yuta Tanaka,² and Shinji Tsuneyuki¹

¹*Department of Physics, The University of Tokyo,
7-3-1 Hongo, Bunkyo-ku, Tokyo 113-0033, Japan*

²*Central Technical Research Laboratory, ENEOS Corporation, 8,
Chidoricho, Naka-ku, Yokohama, Kanagawa 231-0815, Japan*

(Dated: February 12, 2025)

To verify “hot superconductivity” recently proposed in lanthanum hydride-based compounds, we explored thermodynamically stable and superconducting phases in the lanthanum (La)-platinum (Pt)-hydrogen (H) ternary system at 20 GPa using an evolutionary construction scheme of a formation-enthalpy convex hull, universal neural network potential calculations, and density functional theory calculations. Although we found no evidence of the hot superconductivity in this ternary system, we predicted a unique compound, LaPtH₆, which has equilateral triangular H₃ units nearly forming a two-dimensional kagome lattice between La and Pt layers and shows the superconductivity at 18.67 K. This structure is dynamically stable from ambient pressure to at least 200 GPa and the superconducting critical temperature increases from 13.51 to 40.63 K.

I. INTRODUCTION

Metallic hydrides have attracted much attention as potential candidates for room-temperature superconductivity^{1,2}. In 2015, high-temperature superconductivity was observed in sulfur hydride (S-H) under high pressure, and the superconducting critical temperature (T_c) reaches 203 K at pressure of 155 GPa. This discovery triggered further theoretical studies on stoichiometry, crystal structure, and superconductivity in the S-H system under high pressure^{3–8}, and it was clarified that H₃S compound emerges in the high T_c phase⁹. Moreover, in 2018 and 2019, higher T_c was experimentally discovered in lanthanum hydride (La-H) under high pressure. First, LaH₁₀ compound was predicted to emerge as a stable phase showing high T_c ^{10,11}, and then it was experimentally confirmed to show T_c of 250–260 K at 170–190 GPa^{12,13}. In addition, it is also interesting how the H atoms behave in crystal structure. In H₃S, the H₂ molecules are completely dissociated and form covalent bonds with the S atoms. On the other hand, in LaH₁₀, the H₂ molecules are weakly connected and form a cage structure surrounding the La atom.

Many first-principles calculations have predicted the superconductivity in binary hydrides under high pressure with respect to more than 60 elements¹⁴, whereas room-temperature superconductivity has not been obtained in the binary hydrides. Therefore, ternary hydrides are gathering attention as the next stage for the exploration of higher T_c . In 2019, Sun *et al.* predicted from first-principles calculations that Li₂MgH₁₆ shows T_c of 475 K at 250 GPa¹⁵. In 2020, Sun *et al.* and Cui *et al.* predicted that the insertion of CH₄ into H₃S causes the dynamical stabilization of the high T_c phase at lower pressures and CSH₇ shows the T_c values of 100–190 K in pressure range of 100–200 GPa^{16,17}.

Inspired by these theoretical results, experimentalists have explored novel ternary or multinary hydrides showing higher T_c at lower pressures. In 2022, Grockowiak *et al.* reported “hot superconductivity” in ternary or

multinary compounds based on the La-H system¹⁸. The authors claim that T_c is increased to 550 K by subsequent thermal excursion to high temperatures, which might be induced by the reaction of La-H with other materials existing in the sample chamber of the diamond anvil cell (DAC). Their experimental condition indicates that the candidates for the other materials are nitrogen (N) and boron (B) derived from ammonia borane used as hydrogen source, platinum (Pt), gold (Au), and gallium (Ga) from electrodes, etc. However, in first-principles calculations, the evidence of the hot superconductivity has not been found in the La-N-H, La-B-H, and La-Ga-H systems in high pressure region above 100 GPa^{19,20} and the La-N-H system at lower pressure of 20 GPa²¹.

In this paper, assuming that La-H is reacted with Pt, we searched for thermodynamically stable and metastable phases and superconducting phases in the La-Pt-H ternary system using an evolutionary construction scheme (ECS) of a formation-enthalpy convex hull, universal neural network potential calculations, and density functional theory calculations. We set the pressure value at 20 GPa, which is easily generated by multi-anvil apparatus widely used in the field of materials science. Since the multi-anvil apparatus can accommodate much larger samples than DAC, synthesis of hydrides, x-ray diffraction measurements, superconductivity measurements (zero resistance and Meissner effect), and data analysis are much easier than those in DAC. Therefore, calculated results can immediately be validated by many experimental groups.

II. COMPUTATIONAL DETAILS

The experimental findings of the metallic hydrides with high T_c have all been motivated by theoretical crystal structure predictions^{22–25}, whereas the search for thermodynamically stable phases in ternary systems is computationally expensive. To overcome this problem, we performed fast and accurate search for stable phases by

combining ECS of a formation-enthalpy convex hull²⁶, universal neural network potential calculations by Matlantis²⁷, and density functional theory calculations by the Quantum ESPRESSO (QE) code²⁸. The details of the method are given in Ref. [21].

For the calculations by QE, we used the generalized gradient approximation by Perdew, Burke and Ernzerhof²⁹ for the exchange-correlation functional, and the Rabe-Rappe-Kaxiras-Joannopoulos ultrasoft pseudopotential³⁰. The energy cutoff was set at 80 Ry for the wave function and 640 Ry for the charge density. We increased the number of the k -point samplings in the Brillouin zone for optimization until the formation enthalpy is sufficiently converged. For the calculations on Matlantis, we used the PrePreferred Potential (PPF) v.3.0.0³¹. and the L-BFGS optimization algorithm³². We performed the constant-pressure variable-cell optimization at 20 GPa for the created structures. The space groups of the predicted structures were assigned using FYNDSYM³³.

The superconducting T_c was calculated using the Allen-Dynes modified McMillan formula³⁴,

$$T_c = \frac{f_1 f_2 \omega_{\log}}{1.2} \exp \left[-\frac{1.04(1 + \lambda)}{\lambda - \mu^*(1 + 0.62\lambda)} \right]. \quad (1)$$

The parameters, λ and ω_{\log} , are electron-phonon coupling constant and logarithmic-averaged phonon frequency, respectively, which represent a set of characters for the phonon-mediated superconductivity. f_1 and f_2 are correlation factors for the systems showing large λ . To obtain these parameters, we performed the phonon calculations implemented in the QE code. The effective screened Coulomb repulsion constant μ^* was assumed to be 0.10, which has been considered to be a reasonable value for hydrides. The k - and q -point grids for the calculations are listed in Table S1 in the Supplemental Material (SM)³⁵.

III. RESULTS

Figure 1a shows the convex hull diagram of the formation enthalpy for the La-Pt-H system ($\text{La}_x\text{Pt}_y\text{H}_{1-x-y}$; $0 \leq x \leq 1$, $0 \leq y \leq 1$) at the 10th generation obtained by the QE optimization after the screening by Matlantis (See Figs. S1 and S2 in SM for the convex hull diagram obtained by Matlantis only³⁵). In this figure, the convex hull is projected on the xy plane, viewed along the z axis showing the formation enthalpy. The lines and their intersections show the edges and vertices of the convex hull, respectively: the vertices correspond to thermodynamically stable compounds at 20 GPa. The small dots are compositions created by ECS. We obtained twenty thermodynamically stable compounds as shown in the figures. Figure 1b shows only the moderately metastable compounds whose enthalpy difference (ΔH) to the convex hull is less than 4.4 mRy/atom. According to a large-scale data-mining study of the Ma-

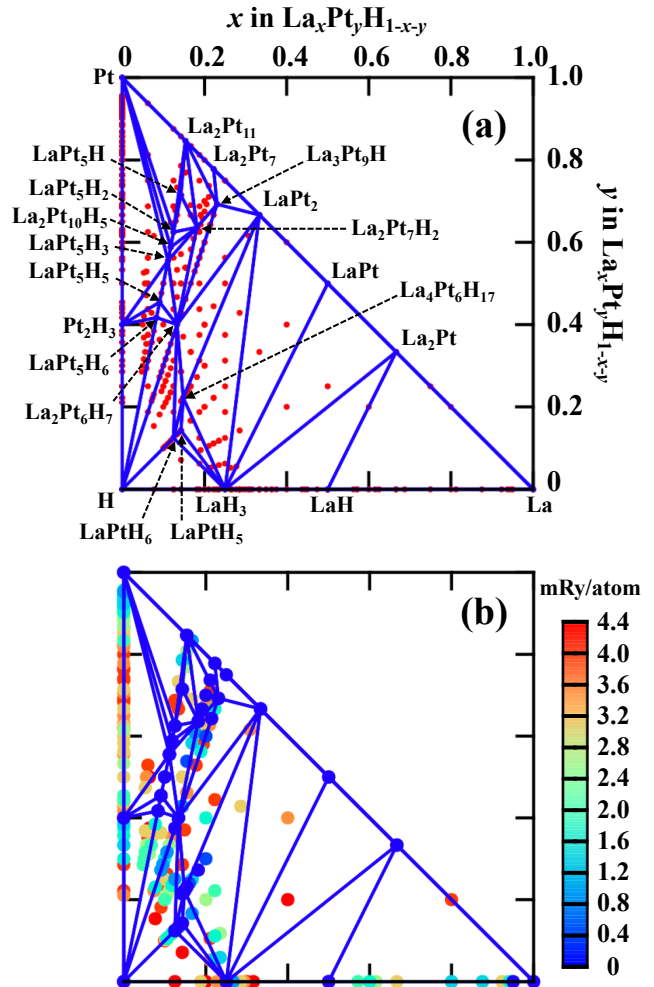


FIG. 1: Formation-enthalpy convex hull diagram of the La-Pt-H system ($\text{La}_x\text{Pt}_y\text{H}_{1-x-y}$) at 20 GPa, obtained by QE. The convex hull is projected on the xy plane, and the vertices (the intersections of the lines) correspond to thermodynamically stable compounds: (a) All the compounds investigated in this study and (b) moderately metastable compounds with ΔH less than 4.4 mRy/atom.

terials Project in Ref. [36], metastable materials with $\Delta H < 70 \text{ meV/atom} = 5.15 \text{ mRy/atom}$ predicted by DFT calculations are promising candidates to be synthesized by experimental techniques. Hence, we set the upper limit of ΔH at 4.4 mRy/atom. The compounds with small ΔH are concentrated in the Pt-rich region including the line connecting between LaPt_5H_6 and $\text{La}_2\text{Pt}_{11}$.

Next we compare the results obtained by ECS with the experimental and theoretical ones reported earlier. On the binary La-H line, we have already confirmed that the experimental results are well reproduced by our search²¹. On the binary Pt-H line, previous first-principles calculations predict that PtH compound with a tetragonal $I4m2$ structure is stabilized against decomposition into Pt and H at 21 GPa³⁷. On the other hand, our calculations predict that PtH takes an orthorhombic $Imm2$

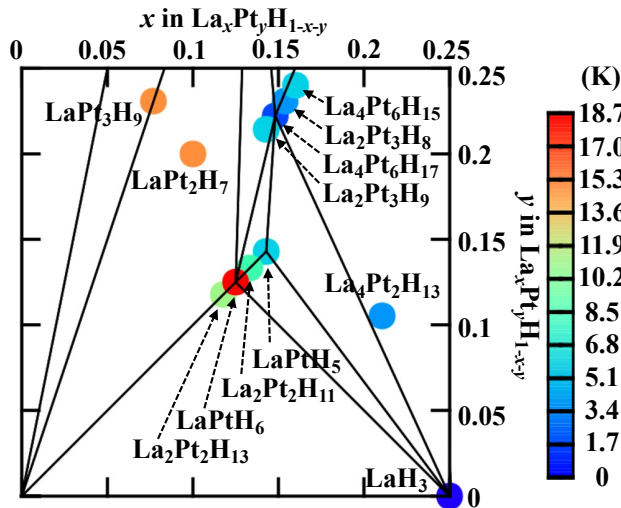


FIG. 2: Superconducting T_c data for stable and moderately metastable compounds in hydrogen rich region at 20 GPa. The color of the circle represents the magnitude of the T_c value.

structure as the most stable one, whose enthalpy is lower by 1.1 mRy/atom than that of $I\bar{4}m2$ at 20 GPa. However, PtH is thermodynamically unstable at 20 GPa because Pt_2H_3 with a trigonal $R\bar{3}m$ structure emerges as a vertex of the convex hull. Experimental studies show that unknown Pt-H phases emerge at 21 GPa and a single phase of PtH with a hexagonal $P6_3/mmc$ structure is obtained at 42 GPa³⁸. Therefore, if Pt_2H_3 is considered as a phase of the unknown phases observed in the range of 21–42 GPa, our results seem to be consistent with the experimental ones.

Following the convex hull diagram predicted by ECS, we investigated the superconductivity for some compounds which are metallic and dynamically stable. While the La-Pt-H system basically shows weak superconductivity at 20 GPa (see Table S2 and Fig. S3 in SM³⁵), four ternary compounds in hydrogen rich region show the superconducting T_c values above 10 K. Figure 2 shows the T_c values in hydrogen rich region, $0 \leq x \leq 0.25$ and $0 \leq y \leq 0.25$. The superconducting compounds are classified into five types following the ratio of La and Pt: (i) 1:1, (ii) 2:3, (iii) 1:2, (iv) 1:3, and (v) 2:1 types. $LaPtH_6$ of the 1:1 type shows the highest T_c of all the compounds predicted in this study. The T_c value is 18.67 K ($\lambda = 0.7014$ and $\omega_{log} = 511.7$ K) and is higher by about 4 K than the highest T_c in the La-N-H system at the same pressure predicted earlier²¹. As listed in Table I, the superconductivity is weakened by increase or decrease of the hydrogen concentration of $LaPtH_6$ within the 1:1 type. $LaPt_2H_7$ of the 1:2 type and $LaPt_3H_9$ of the 1:3 type show the T_c value of about 14.6 K, which is the second highest T_c of all the predicted compounds. The 2:3 and 2:1 types show the T_c values from 2.58 through 6.40 K. The structure data (CIF files) of all the super-

TABLE I: Superconductivity data of ternary compounds in the La-Pt-H system, predicted by the evolutionary construction scheme of a formation-enthalpy convex hull. ΔH , λ , ω_{log} , and T_c are the enthalpy difference to the convex hull in the unit of mRy/atom, the electron-phonon coupling constant, the logarithmic-averaged phonon frequency in the unit of K, and the superconducting critical temperature in the unit of K, respectively.

La:Pt	Compound	Structure	ΔH	λ	ω_{log}	T_c
1:1	$La_2Pt_2H_{13}$	$P1$	0.74	0.6150	449.5	11.46
	$LaPtH_6$	$R\bar{3}m$	0	0.7014	511.7	18.67
	$La_2Pt_2H_{11}$	Cm	0.78	0.5823	463.3	9.98
	$LaPtH_5$	$C2/m$	0	0.4942	551.6	6.56
	$La_4Pt_6H_{17}$	$P1$	0	0.4364	379.3	2.58
2:3	$La_2Pt_3H_9$	$P1$	0.34	0.5569	343.3	6.38
	$La_2Pt_3H_8$	$P1$	0.12	0.5217	307.3	4.52
	$La_4Pt_6H_{15}$	$P1$	0.70	0.6039	265.5	6.40
	$La_2Pt_3H_9$	$P1$	0.34	0.5569	343.3	6.38
1:2	$LaPt_2H_7$	$P1$	2.11	0.7879	305.3	14.59
1:3	$LaPt_3H_9$	$P1$	1.95	0.8158	284.0	14.61
2:1	$La_4Pt_2H_{13}$	$P1$	3.78	0.5277	324.9	4.98

conducting compounds are provided in SM³⁵.

Here, we focus on $LaPtH_6$ showing the highest T_c . This compound has the highest concentration of hydrogen of all the stable compounds predicted in this study and forms a simple but unique crystal structure. Figure 3a shows the structure of $LaPtH_6$, assigned as a trigonal $R\bar{3}m$. This structure has octahedral PtH_6 units, and Bader charge analysis shows that the La atom and the PtH_6 unit are positively and negatively charged, respectively (Table S3 and Fig. S4 in SM). The positively charged La ions and the negatively charged PtH_6 units individually form triangular lattice layers, and they are stacked along the c axis with the order of A(La)-B(PtH_6)-C(La)-A(PtH_6)-B(La)-C(PtH_6). Note that A, B, and C are the same as the layer positions describing the hexagonal close-packed structure (A-B) or the face-centered cubic structure (A-B-C) and a component forming each layer is shown in parentheses. As shown in Fig. 3b, three H atoms form an equilateral triangle like so-called triatomic hydrogen, H_3 . The H-H bond length of an H_3 unit (R_H) is 1.87Å and the nearest neighbor distance between the H_3 units (R_{H_3}) is 2.55Å, in which the atomic alignment is similar to a two-dimensional kagome lattice. The center of the mass of an H_3 unit occupies the layer position other than those of the neighboring layers, e.g., if an H_3 unit is intercalated between the A(La) and B(Pt) layers, the center of the mass occupies the C position. In addition, the H_3 units in the same layer point the same direction: parallel or anti-parallel to the $\mathbf{a} - \mathbf{b}$ direction (Fig. 3b). If the former and latter are defined as R and L, respectively, the structure of $LaPtH_6$ is also represented as the stacking structure with the order of A(La)-C(H_3 :L)-B(Pt)-A(H_3 :R)-C(La)-B(H_3 :L)-A(Pt)-

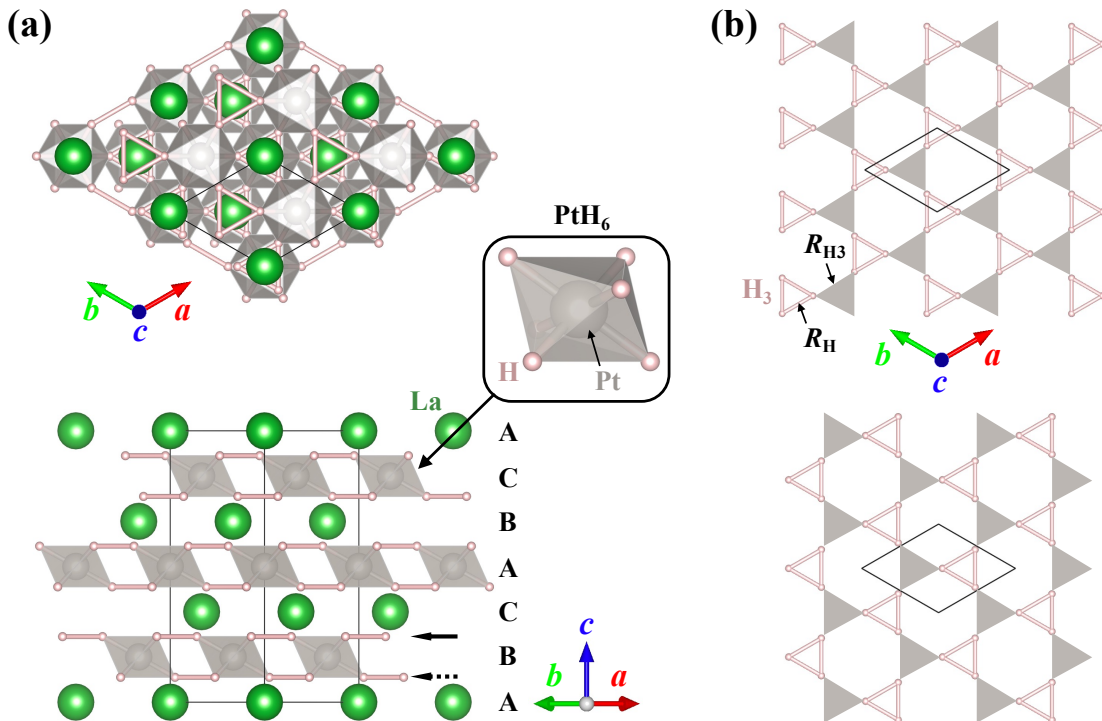


FIG. 3: (a) Crystal structure of LaPtH₆, assigned as a trigonal $R\bar{3}m$. Octahedral PtH₆ units are formed, and the La layer and the PtH₆ layer are stacked along the c axis with the order of A(La)-B(PtH₆)-C(La)-A(PtH₆)-B(La)-C(PtH₆). The solid lines show the unit cell. (b) Views of the H layers. The upper and lower figures correspond to the layers indicated by the solid and dotted horizontal arrows in (a), respectively. The H₃ units nearly form two-dimensional kagome lattices, in which R_H and R_{H3} represent the H-H bond length of the H₃ unit and the nearest neighbor distance between the H₃ units, respectively. The shaded triangles show the facets of the octahedron. The structure was drawn with VESTA³⁹.

C(H₃:R)-B(La)-A(H₃:L)-C(Pt)-B(H₃:R) along the c axis. In contrast, LaH₃ considered as an analog of LaPtH₆ has no H₃ unit, and the H atoms form an extensive covalent network with the bond length of 2.27Å (Fig. S5 in SM³⁵).

Figure 4 shows the electronic band structure and the density of states (DOS) for $R\bar{3}m$ LaPtH₆ at 20 GPa. This compound has a band structure like electron-doped insulators, in which the Fermi level lies in the bands immediately above the gap. The bottom panel of this figure shows the partial DOS. The 5*d* states of La and Pt [La(5*d*) and Pt(5*d*)] dominantly contribute to the electronic states at the Fermi level. The hydrogen 1*s* [H(1*s*)] also shows a large contribution to the electronic states at the Fermi level, which causes the enhancement of the superconductivity. In hydrides based on lanthanides like LaH₁₀ at 250 GPa, the 4*f* states of La [La(4*f*)] dominantly contribute to the states at the Fermi level, which causes the high T_c superconductivity^{11,40}. However, in the case of LaPtH₆, the contribution of La(4*f*) is smaller than those of La(5*d*), Pt(5*d*), and H(1*s*). Figure 5 shows the phonon dispersion and the cumulative electron-phonon coupling constant $\lambda(\omega)$ of LaPtH₆, where ω represents the phonon frequency. The low frequency modes below 164 cm⁻¹ contribute to 41.2% of the

total λ value, 0.7014. In addition, the high-frequency modes above 1550 cm⁻¹, related to vibrations of the H₃ units, also contribute to 16.8% of λ . The phonon of $R\bar{3}m$ LaPtH₆ is robust against pressure and has no imaginary frequency from 0 to at least 200 GPa (Fig. S6 in SM³⁵). Thus, once $R\bar{3}m$ LaPtH₆ is synthesized under high pressure, it can be quenched to ambient pressure. R_H is almost equal to R_{H3} at 0 GPa, in which the H atoms nearly form a complete two-dimensional kagome lattice. As pressure increases, the PtH₆ units approach each other and the size of the H₃ unit becomes smaller. In contrast, R_{H3} increases to about 2.6Å (Table II). We calculated the T_c values and found that T_c increases from 13.51 to 40.63 K as pressure increases from 0 to 200 GPa (Table II). These results suggest that LaPtH₆ can not explain the hot superconductivity experimentally observed at 180 GPa.

IV. DISCUSSIONS AND CONCLUSIONS

To verify the hot superconductivity reported earlier, we explored thermodynamically stable and metastable phases in the ternary La-Pt-H system at 20 GPa using ECS, the universal neural network potential calculations

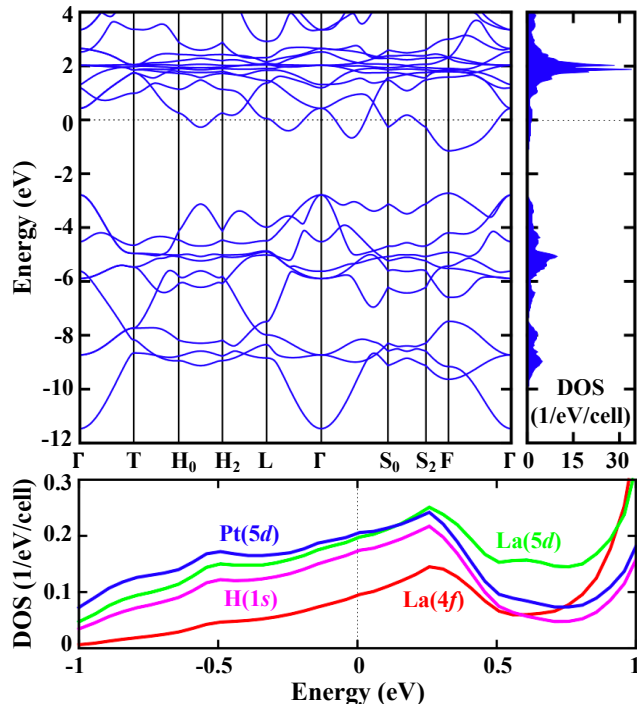


FIG. 4: Electronic band dispersion and density of states (DOS) of LaPtH₆ at 20 GPa (upper), and partial DOS in the vicinity of the Fermi level (lower). La(5*d*), La(4*f*), Pt(5*d*), and H(1*s*) represent the 5*d* states of La, the 4*f* states of La, the 5*d* states of Pt, and the 1*s* states of H, respectively. The Fermi level is set to zero.

TABLE II: Pressure (*P*) dependence of superconductivity for *R*3*m* LaPtH₆. The parameters *R*_H and *R*_{H3} show the H-H bond length of an H₃ unit and the nearest neighbor distance between the H₃ units in the same layer, respectively.

<i>P</i> (GPa)	<i>R</i> _H (Å)	<i>R</i> _{H3} (Å)	λ	ω_{\log} (K)	<i>T</i> _c (K)
0	2.23	2.43	0.7893	282.1	13.51
20	1.87	2.55	0.7014	511.7	18.67
50	1.62	2.63	0.6628	771.6	24.32
100	1.42	2.66	0.6856	942.4	32.43
150	1.30	2.66	0.7121	1016.7	38.48
200	1.23	2.64	0.7182	1051.3	40.63

by Matlantis, and the DFT calculations by QE. While new superconducting compounds were predicted in the hydrogen-rich region, the highest *T*_c value is 18.67 K obtained in LaPtH₆, which is higher by about 4 K than the highest *T*_c in the La-N-H system at the same pressure. Although we found no evidence of the hot superconductivity in this study, we found LaPtH₆ with a simple but unique crystal structure, in which the equilateral triangular H₃ units almost form a two-dimensional kagome lattice between the La and Pt layers. This behavior of

the H atoms is significantly different from the S-H and La-H systems cases: Dissociation of the H₂ molecules in

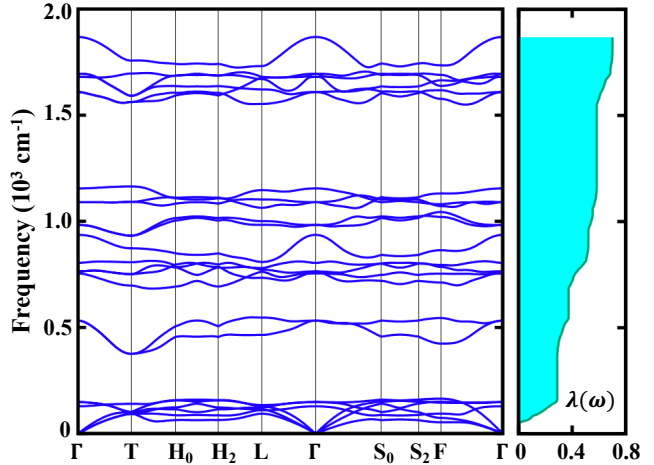


FIG. 5: Phonon dispersion and cumulative electron-phonon coupling constant $\lambda(\omega)$ of LaPtH₆ at 20 GPa. ω represents phonon frequency.

S-H and weak connection of the H₂ molecules in La-H. We also found that the vibration modes of the H₃ units contribute to the enhancement of the superconductivity. Since the phonon of LaPtH₆ with the H₃ units is robust against pressure and shows no imaginary frequency over a wide range from ambient pressure to at least 200 GPa, it is quite possible that the compound is synthesized by experiments and is quenched to ambient condition.

The existence of triatomic hydrogen, H₃, was first proposed by Thomson in 1911⁴¹, and spectroscopic lines of neutral H₃ was first observed by Herzberg in 1979⁴² via many experimental and theoretical studies⁴³. A neutral H₃ molecule is unstable and breaks up in under a microsecond after the formation, and an H₃⁺ ion is one of the most abundant molecular ions in the universe, which is believed to have played a crucial role in the cooling of early stars in the history of the universe. In addition, a kagome lattice consisting of the H atoms may exhibit novel physical properties connected with the geometrical frustration. Thus, our predicted LaPtH₆ could be an excellent model for exploring these phenomena.

Acknowledgments

This work was supported by JSR-UTokyo Collaboration Hub, CURIE, and JSPS KAKENHI under Grant-in-Aid for Scientific Research (C) (23K03316), Scientific Research (B) (24K00544), and Scientific Research (S) (20H05644). A part of the computation was performed using the facilities of the Supercomputer Center, the Institute for Solid State Physics, the University of Tokyo.

- * Electronic address: takahiro.ishikawa@phys.s.u-tokyo.ac.jp
- ¹ N. W. Ashcroft, Phys. Rev. Lett. **21**, 1748 (1968).
 - ² N. W. Ashcroft, Phys. Rev. Lett. **92**, 187002 (2004).
 - ³ D. Duan, X. Huang, F. Tian, D. Li, H. Yu, Y. Liu, Y. Ma, B. Liu, and T. Cui, Phys. Rev. B **91**, 180502(R) (2015).
 - ⁴ I. Errea, M. Calandra, C. J. Pickard, J. Nelson, R. J. Needs, Y. Li, H. Liu, Y. Zhang, Y. Ma, and F. Mauri, Phys. Rev. Lett. **114**, 157004 (2015).
 - ⁵ R. Akashi, M. Kawamura, S. Tsuneyuki, Y. Nomura, and R. Arita, Phys. Rev. B **91**, 224513 (2015).
 - ⁶ I. Errea, M. Calandra, C. J. Pickard, J. R. Nelson, R. J. Needs, Y. Li, H. Liu, Y. Zhang, Y. Ma, and F. Mauri, Nature **532**, 81 (2016).
 - ⁷ T. Ishikawa, A. Nakanishi, K. Shimizu, H. Katayama-Yoshida, T. Oda, and N. Suzuki, Sci. Rep. **6**, 23160 (2016).
 - ⁸ R. Akashi, W. Sano, R. Arita, and S. Tsuneyuki, Phys. Rev. Lett. **117**, 075503 (2016).
 - ⁹ M. Einaga, M. Sakata, T. Ishikawa, K. Shimizu, M. I. Eremets, A. P. Drozdov, I. A. Troyan, N. Hirao, and Y. Ohishi, Nat. Phys. **12**, 835 (2016).
 - ¹⁰ F. Peng, Y. Sun, C. J. Pickard, R. J. Needs, Q. Wu, and Y. Ma, Phys. Rev. Lett. **119**, 107001 (2017).
 - ¹¹ H. Liu, I. I. Naumov, R. Hoffmann, N. W. Ashcroft, and R. J. Hemley, Proc. Natl. Acad. Sci. USA **114**, 6990 (2017).
 - ¹² M. Somayazulu, M. Ahart, A. K. Mishra, Z. M. Geballe, M. Baldini, Y. Meng, V. V. Struzhkin, and R. J. Hemley, Phys. Rev. Lett. **122**, 027001 (2019).
 - ¹³ A. P. Drozdov, P. P. Kong, V. S. Minkov, S. P. Besedin, M. A. Kuzovnikov, S. Mozaffari, L. Balicas, F. F. Balakirev, D. E. Graf, V. B. Prakapenka, et al., Nature **569**, 528 (2019).
 - ¹⁴ T. Ishikawa, T. Miyake, and K. Shimizu, Phys. Rev. B **100**, 174506 (2019).
 - ¹⁵ Y. Sun, J. Lv, Y. Xie, H. Liu, and Y. Ma, Phys. Rev. Lett. **123**, 097001 (2019).
 - ¹⁶ Y. Sun, Y. Tian, B. Jiang, X. Li, H. Li, T. Iitaka, X. Zhong, and Y. Xie, Phys. Rev. B **101**, 174102 (2020).
 - ¹⁷ W. Cui, T. Bi, J. Shi, Y. Li, H. Liu, E. Zurek, and R. J. Hemley, Phys. Rev. B **101**, 134504 (2020).
 - ¹⁸ A. D. Grockowiak, M. Ahart, T. Helm, W. A. Coniglio, R. Kumar, K. Glazyrin, G. Garbarino, Y. Meng, M. Oliff, V. Williams, et al., Front. Electron. Mater. **2**, 837651 (2022).
 - ¹⁹ Y. Ge, F. Zhang, and R. J. Hemley, Phys. Rev. B **104**, 214505 (2021).
 - ²⁰ S. Di Cataldo, W. von der Linden, and L. Boeri, npj Comput. Mater. **8**, 2 (2022).
 - ²¹ T. Ishikawa, Y. Tanaka, and S. Tsuneyuki, Phys. Rev. B **109**, 094106 (2024).
 - ²² A. R. Oganov and C. W. Glass, J. Chem. Phys. **124**, 244704 (2006).
 - ²³ A. R. Oganov, Y. Ma, A. O. Lyakhov, M. Valle, and C. Gatti, Rev. Mineral. Geochem. **71**, 271 (2010).
 - ²⁴ Y. Wang, J. Lv, L. Zhu, and Y. Ma, Phys. Rev. B **82**, 094116 (2010).
 - ²⁵ C. J. Pickard and R. J. Needs, J. Phys.: Condens. Matter **23**, 053201 (2011).
 - ²⁶ T. Ishikawa and T. Miyake, Phys. Rev. B **101**, 214106 (2020).
 - ²⁷ Matlantis (<https://matlantis.com/>), software as a service style material discovery tool.
 - ²⁸ P. Giannozzi, S. Baroni, N. Bonini, M. Calandra, R. Car, C. Cavazzoni, D. Cereso, G. L. Chiarott, M. Cococcioni, I. Dabo, et al., J. Phys.: Condens. Matter **21**, 395502 (2009).
 - ²⁹ J. P. Perdew, K. Burke, and M. Ernzerhof, Phys. Rev. Lett. **77**, 3865 (1996).
 - ³⁰ A. M. Rappe, K. M. Rabe, E. Kaxiras, and J. D. Joannopoulos, Phys. Rev. B **41**, 1227 (1990).
 - ³¹ S. Takamoto, C. Shinagawa, D. Motoki, K. Nakago, W. Li, I. Kurata, T. Watanabe, Y. Yayama, H. Iriguchi, Y. Asano, et al., Nat. Commun. **13**, 2991 (2022).
 - ³² D. C. Liu and J. Nocedal, Math. Program. B **45**, 503 (1989).
 - ³³ H. T. Stokes and D. M. Hatch, J. Appl. Cryst. **38**, 237 (2005).
 - ³⁴ P. B. Allen and R. C. Dynes, Phys. Rev. B **12**, 905 (1975).
 - ³⁵ See Supplemental Material at [URL will be inserted by publisher] for calculation accuracy of Matlantis and calculation conditions and superconductivity data for stable and moderately metastable compounds in the La-Pt-H system at 20 GPa.
 - ³⁶ W. Sun, S. T. Dacek, S. P. Ong, G. Hautier, A. Jain, W. D. Richards, A. C. Gamst, K. A. Persson, and G. Ceder, Sci. Adv. **2**, e1600225 (2016).
 - ³⁷ D. Y. Kim, R. H. Scheicher, C. J. Pickard, R. J. Needs, and R. Ahuja, Phys. Rev. Lett. **107**, 117002 (2011).
 - ³⁸ T. Scheler, O. Degtyareva, M. Marqués, C. L. Guillaume, J. E. Proctor, S. Evans, and E. Gregoryanz, Phys. Rev. B **83**, 214106 (2011).
 - ³⁹ K. Momma and F. Izumi, J. Appl. Crystallogr. **44**, 1272 (2011).
 - ⁴⁰ E. Plekhanov, Z. Zhao, F. Macheda, Y. Wei, N. Bonini, and C. Weber, Phys. Rev. Research **4**, 013248 (2022).
 - ⁴¹ J. J. Thomson, Philosophical Magazine **21**, 225 (1911).
 - ⁴² G. Herzberg, J. Chem. Phys. **70**, 4806 (1979).
 - ⁴³ H. Kragh, Centaurus **53**, 257 (2011).